Research article

Carbon Future

Metal-free carbon-nitrogen@carbon-type hybrid electrocatalysts for peroxide-producing oxygen reduction reaction

Bin Wu[1,2], Dulce M. Morales[3,4], Mingren Liu[5,6], Dongjiu Xie[7], Ping Feng[7], Yan Lu[7], Marcel Risch[3], Martin Oschatz[5,6], and Tristan Petit[1] ✉

[1] *Young Investigator Group Nanoscale Solid-Liquid Interfaces, Helmholtz-Zentrum Berlin für Materialien und Energie GmbH, 12489 Berlin, Germany*
[2] *Institute of Physics, Humboldt University Berlin, 12489 Berlin, Germany*
[3] *Nachwuchsgruppe Gestaltung des Sauerstoffentwicklungsmechanismus, Helmholtz-Zentrum Berlin für Materialien und Energie GmbH, 14109 Berlin, Germany*
[4] *Engineering and Technology Institute Groningen (ENTEG), Faculty of Science and Engineering, University of Groningen, 9747 AG, Groningen, Netherlands*
[5] *Friedrich-Schiller-University Jena, Institute for Technical Chemistry and Environmental Chemistry, 07743 Jena, Germany*
[6] *Center for Energy and Environmental Chemistry Jena (CEEC Jena), 07743 Jena, Germany*
[7] *Institute of Electrochemical Energy Storage, Helmholtz-Zentrum Berlin für Materialien und Energie, 14109 Berlin, Germany*

Cite This: *Carbon Future* **2024**, *1*, 9200022

Read Online

ABSTRACT: Hydrogen peroxide (H_2O_2) is a widely utilized chemical in environmental cleaning, medical disinfection, and chemical engineering. Compared to the traditional anthraquinone oxidation method, the electrocatalytic oxygen reduction reaction (ORR) has become a promising alternative following the trends towards decentralized production schemes for base chemicals as well as the implementation of renewable energy sources to drive chemical reactions. ORR is attractive for the production of H_2O_2 due to its environmental friendliness, safety, and reliability. However, its wider application is still restricted by the sluggish reaction kinetics and low selectivity due to the competitive reaction of the oxygen reduction to H_2O. In this context, nitrogen-rich carbon electrocatalysts with tunable adsorption properties and high electrical conductivity are promising materials for improved selectivity. A precise tailoring of their chemical structure is however required to embed peroxide-producing catalytic sites within a conductive environment. Herein, a metal-free carbon-nitrogen (CN)-type nanoporous carbon loaded onto a carbon matrix (CN@C) was designed as an ORR catalyst for highly selective peroxide synthesis in alkaline media. An average electron transfer number of 2.2 has been determined by the Koutecký–Levich analysis, indicating that CN@C materials exhibit a high selectivity for electrochemical H_2O_2 synthesis.

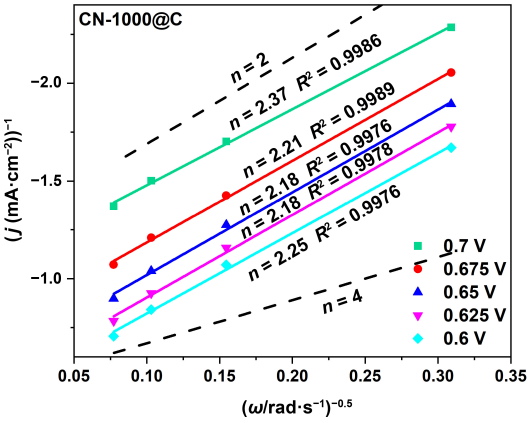

KEYWORDS: hybrids, electrocatalysts, oxygen reduction reaction, metal-free electrocatalyst, nanoporous carbon

1 Introduction

Hydrogen peroxide (H_2O_2) is an environmentally friendly, powerful oxidant widely applied across diverse fields, including wastewater treatment, industrial bleaching, chemical synthesis, and medical disinfection[1–3]. The industrial-scale production of H_2O_2 currently relies on the anthraquinone oxidation-reduction process, which is energy-intensive and generates significant waste[4]. As this is a multi-step process, it demands complex facilities, as well as pricey palladium hydrogenation catalysts that produce a considerable number of organic by-products. Furthermore, the storage, handling, and transport of the produced H_2O_2 causes additional expenses and hazards. A more sustainable solution to address the challenges linked to the intricate anthraquinone pathway would be the direct synthesis of H_2O_2 from hydrogen and oxygen. Nevertheless, this method generally requires the use of noble-metal-based catalysts, which in addition to being expensive and scarce, exhibit low catalytic efficiency. Recently, research efforts have been

Received: August 1, 2024; **Revised:** October 8, 2024
Accepted: November 1, 2024

✉Address correspondence to Tristan Petit, tristan.petit@helmholtz-berlin.de

https://doi.org/10.26599/CF.2024.9200022

actively directed towards synthesizing H_2O_2 via the electrocatalytic oxygen reduction reaction (ORR) as a green and secure approach, using abundant, low-cost catalytic materials as well as electricity as the reducing agent which can be extracted from renewable energy sources[4].

The electrocatalytic H_2O_2 synthesis *via* the ORR follows ideally a two-electron transfer pathway in alkaline media: $O_2 + H_2O + 2e^- \rightarrow HO_2^- + OH^-$ [5]. However, designing an ideal reaction platform to produce H_2O_2 is challenging due to the possible competing O_2 reduction to H_2O through the four-electron transfer pathway ($O_2 + 2H_2O + 4e^- \rightarrow 4OH^-$) or the further cleavage of O–O bond in H_2O_2 ($2H_2O_2 \rightarrow 2H_2O + O_2$) [6]. The poor selectivity towards the formation of peroxide species reduces the overall efficiency of the process and, in turn, increases the cost of H_2O_2 production, representing one of the main challenges associated with this synthesis method[7].

The primary focus of prior and current research on electrocatalytic H_2O_2 synthesis has been the development of ORR electrocatalysts that are highly selective to the two-electron transfer ORR pathway[2, 3, 8, 9]. Until now, a variety of materials have been reported as two-electron ORR catalysts, including noble metal/alloys, earth-abundant transition metals, functional carbon materials, hybrid composite materials, and molecular complexes[10, 11]. Despite the progress made in developing peroxide-producing ORR catalysts, their performance in terms of selectivity and hydrogen peroxide production rate as well as further drawbacks such as high costs and limited (electro)chemical stability remain unsatisfactory. Hence, there is still a significant research effort needed to achieve large-scale production of H_2O_2 through the electrocatalytic two-electron ORR pathway with cost-efficient and selective catalysts[4, 5].

Metal-free carbon-based nanoporous materials are considered as potential ORR catalysts due to their affordability, eco-friendliness, excellent electrical conductivity, and high electrocatalytic selectivity[12]. Nevertheless, carbon-based catalysts are prone to carbon corrosion due to a poor electrochemical oxidation resistance. The low corrosion resistance and inevitable active sites loss mostly result from an insufficient level of graphitization[13]. Increasing the graphitization level of carbon substrate improves the electrochemical stability but, on the other hand, results in a hydrophobic character that reduces the accessibility of the catalytic site to water molecules. Heteroatom-doping, particularly with nitrogen, is a promising approach to enhance the electrochemical performance of carbon materials while maintaining or even increasing the hydrophilicity as compared to pristine carbon materials. The increase in electron affinity induced by positively charged carbon sites[14], favors O_2 adsorption and reduction[15, 16]. The resulting nitrogen-rich carbons are particularly promising for the ORR with a variety of reaction pathways proposed[17, 18]. Nevertheless, N-doped porous carbon materials typically exhibit structural heterogeneity, making it challenging to precisely control their chemical architecture[16]. In addition, the instability of nitrogen in most conventional N-containing carbon materials is often observed under electrocatalytic reaction conditions[19]. Therefore, it is a significant challenge to synthesize porous, highly graphitized N-rich carbon frameworks with sufficient active sites to achieve stable ORR with high $2e^-$ selectivity. The synthesis of nitrogen-rich porous carbon materials by controlled condensation of preorganized molecular precursors has recently been reported but have not been considered for ORR so far to our knowledge[20, 21].

Herein, a series of nanoporous nitrogen-rich carbon derived from precursors with a high concentration of pyridinic nitrogen embedded into a matrix of carbon (CN@C) were investigated as ORR electrocatalysts in alkaline media to evaluate their performance for H_2O_2 synthesis. The selective thermal condensation of a hexaazatriphenylene (HAT)-based precursor results in N-rich carbons with a C_2N-type composition, offering porosity and oxidation resistance, synthesized at relatively mild temperatures of 550–700 °C while highly graphitized N-doped carbon materials with nearly similar porosity were obtained at 1000 °C condensation temperature[22]. Different from traditional synthetic processes, such a unique synthesis process from preorganized molecules modifies and restructures the material surface, decorating the porous framework with uniformly distributed, well-defined active sites. HAT is an electron-deficient, rigid, planar aromatic discotic system characterized by exceptional pi–pi stacking capability and significant oxidation resistance, which contributes to a highly polarizable microporous structure and a consequently large accessible surface area.

The nitrogen-containing surface groups serve as active sites with a strong adsorption affinity for molecules such as H_2O and O_2, as recently evidenced by *in situ* soft X-ray spectroscopy[23]. After synthesis, the best-performing catalyst, CN-1000@C, exhibited a highly selective ORR performance with average number of electron transfer of 2.2 determined by the Koutecký–Levich (K–L) analysis through a rotating disk electrode (RDE) setup. Additionally, the catalyst displayed a potential of 0.69 V vs reversible hydrogen electrode (RHE) at a current density of -1 mA·cm^{-2}, and showed high stability over a 100 cycles stability test. The unique metal-free template method to produce CN-type materials with well-defined active sites may allow the rational design of N-rich carbon materials for ORR with high $2e^-$ selectivity.

2 Results and discussion

2.1 CN@C synthesis and material characterizations

Porous CN@C was produced through the direct thermal condensation of hexaazatriphenylene-hexacarbonitrile (HAT-CN) under a nitrogen atmosphere at various temperatures, following its deposition onto a microporous carbon matrix according to a protocol comparable to a previous report[24]. HAT-CN was loaded onto finely ground commercial-grade carbon cloths (Kynol 5092-CC from Kynol Europa GmbH) by liquid phase deposition. This particular hard carbon substrate has been chosen because of the absence of large internal porosity and its high electrical conductivity. The condensed HAT-CN therefore acts as the active carbon materials, and mass-transfer limitation in the hybrid materials is avoided. A critical factor influencing the catalytic process is mass transfer, which dictates the efficiency of reactant supply and product removal at active sites, thereby affecting overall catalytic performance. In gas-involving electrocatalysis, such as oxygen evolution reaction (OER) and ORR, the diffusion behaviour of reactants and products plays a crucial role in these heterogeneous processes. Huang et al. demonstrated that optimizing pore sizes, particularly increasing micropores (< 2 nm), can significantly improve mass transfer[25]. Building on this concept, our designed material, HAT-CN@Carbon cloth, has been confirmed to possess a high micropore volume, as reported by Oschatz et al[22]. These materials can be modified as ORR catalysts to improve the mass transfer during the process, concerning the HAT-CN materials

have a large number of micropores and relatively larger surface area. The resulting materials are hereafter denoted as CN-550@C, CN-700@C, and CN-1000@C corresponding to the synthesis temperatures 550, 700, and 1000 °C, respectively. The nitrogen (oxygen) contents repressed as at.% was previously estimated by X-ray photoelectron spectroscopy (XPS) as 32.7% (3.3%), 29.8% (3.2%), and 7.4% (2.6%) for synthesis at 550, 700, and 1000 °C, respectively, on similarly prepared HAT-CN materials[22]. It is worth noting that, although the ORR catalyst itself is metal-free, we cannot exclude that metal traces contained in the electrolyte may coordinate to surface functional groups[26]. It is more likely to occur on CN-550@C and CN-700@C materials as they are richer in basic nitrogen functionalities which can coordinate metals from the electrolyte. The microstructure of the as-obtained hybrids was examined by scanning electron microscopy (SEM). Individual fragments of the ground carbon fibers with sizes in the range of a few micrometers can be observed for all samples independent of the condensation temperature in Fig. 1 and Supplementary S1. CN-550@C and CN-700@C samples manifest as a cluster of small and flat plates with a smooth surface (Figs. 1a and 1d). In contrast, the fiber-like particles of CN-1000@C have numerous smaller and aggregated particles (Fig. 1g). From the high-resolution transmission electron microscopy (HRTEM) shown in Figs. 1b, 1e, 1h, and Supplementary S1, all materials show an overall disordered carbon microstructure. Energy-dispersive X-ray (EDX) spectroscopy indicates that higher synthesis temperatures lead to lower content of nitrogen in the CN@C materials as shown by elemental mapping images (Figs. 1c, 1f, and 1i), displaying also a uniform distribution of nitrogen on the carbon surface independently of the synthesis temperatures. A detailed analysis of the nitrogen bonding in these porous nitrogen-doped carbon particles based on soft X-ray absorption and photoemission spectroscopies was recently reported[23].

X-ray diffraction (XRD) patterns in Fig. 2a display two main peaks located at around 26° (2θ) and 43° (2θ) which are attributed to (002) and (101) diffraction of graphite-like carbon materials[27]. The (101) reflex of CN-1000@C is slightly sharper than those of CN-550@C and CN-700@C, suggesting a higher degree of graphitization of the deposited CN phase[22]. The XRD reflexes of all CN@C samples are, however, rather broad, which is typical for highly porous and disordered materials. The increased degree of condensation and conjugation within CN-1000@C is expected to improve the electrical conductivity. For further characterization of the sp^2-based carbon structures, Raman spectroscopy was employed. All the spectra are described by two main bands, specifically the D band (breathing mode of sp^2 carbon atoms in aromatic rings) near 1391 cm^{-1} and the G band (sp^2 carbon arranged in chains or rings) around 1587 cm^{-1} as shown in Fig. 2b. The ratio of intensity between the D band and the G band (I_D/I_G) usually correlates to the degree of defectiveness and of graphitization. The higher G-band signal of the CN-1000@C suggests a more graphitic nature of this sample. In general, the higher degree of graphitization ensures that there is a lower number of defects in the particles and hence a higher electrical conductivity. This leads to higher current densities passing through the active catalyst and therefore better electrochemical performance. Yet, the strong contribution from the carbon fiber to the Raman signal does not allow us to draw any definitive conclusion from this ratio on the active carbon particles.

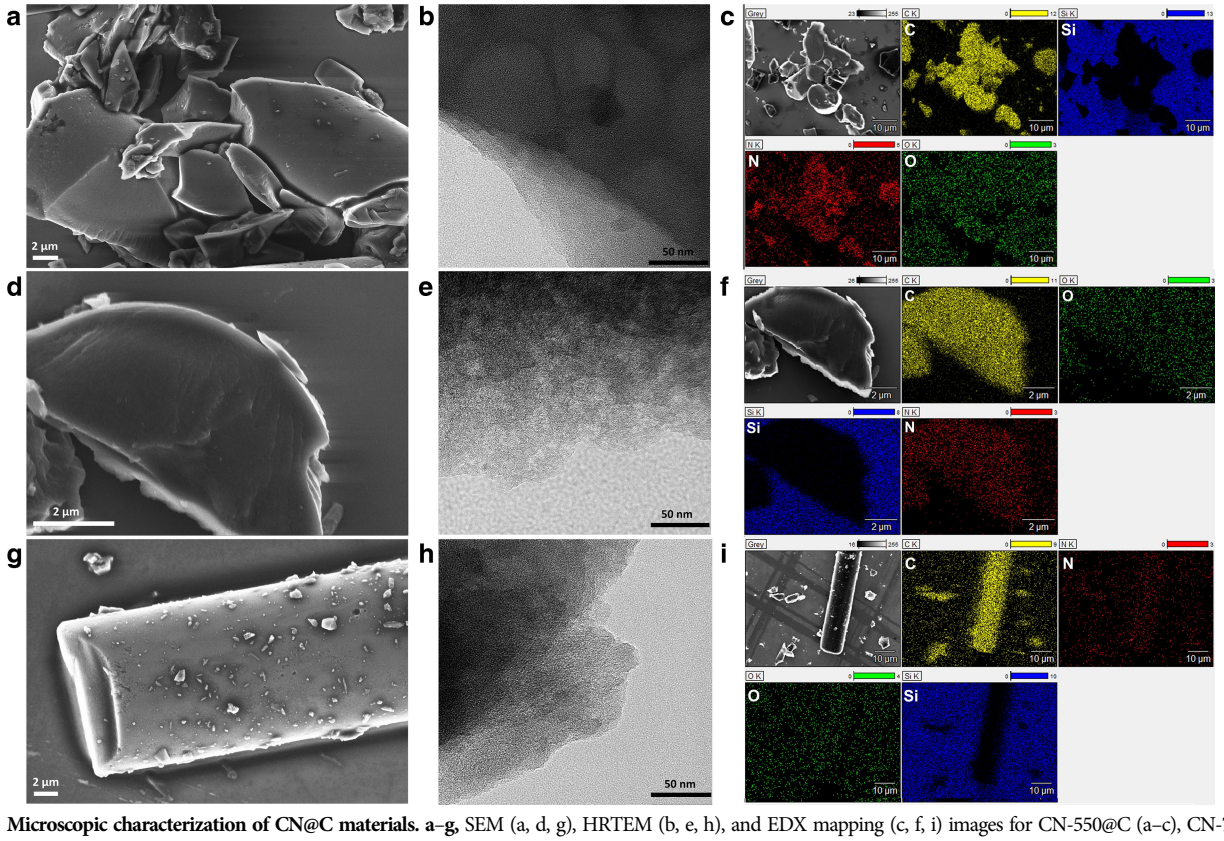

Fig. 1. Microscopic characterization of CN@C materials. a–g, SEM (a, d, g), HRTEM (b, e, h), and EDX mapping (c, f, i) images for CN-550@C (a–c), CN-700@C (d–f), and CN-1000@C (g–i).

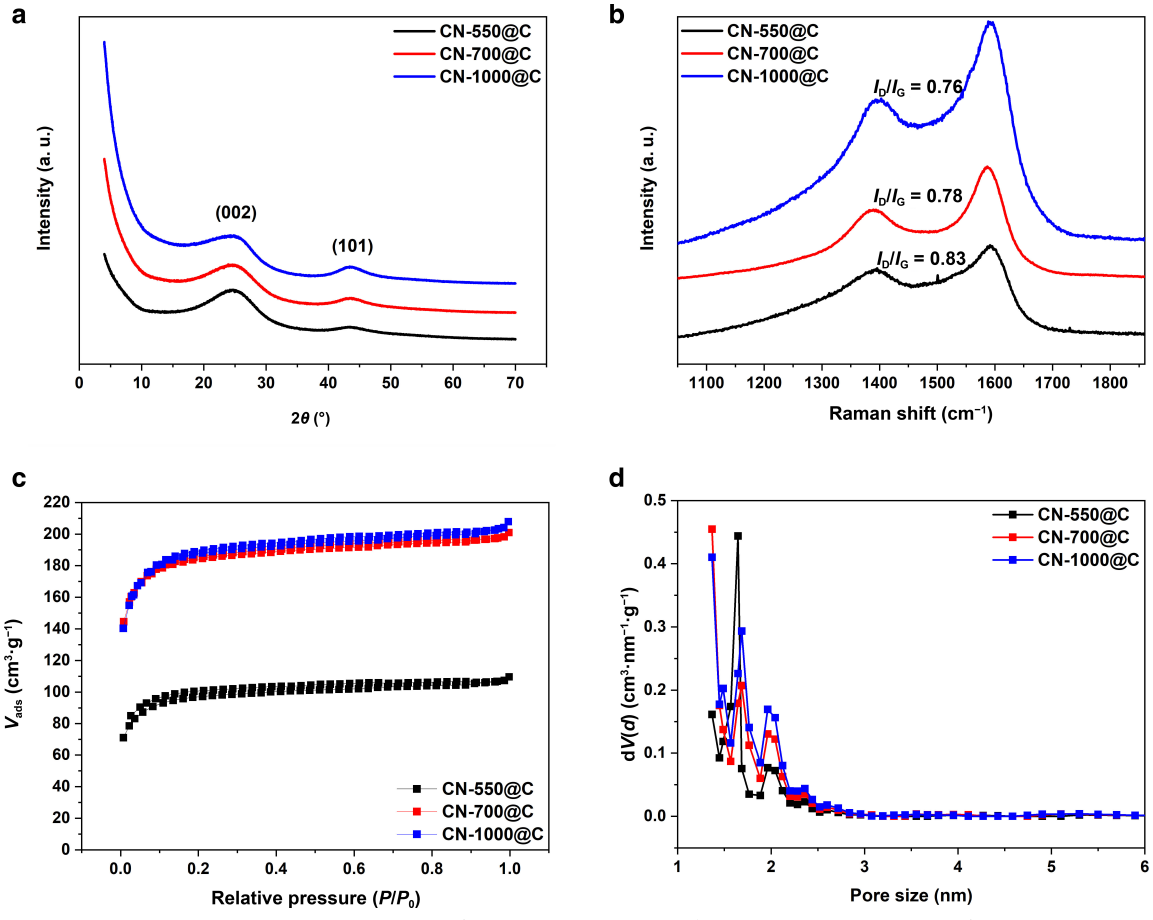

Fig. 2. Structural properties of CN@C materials. a, XRD patterns of CN-550@C, CN-700@C, and CN-1000@C. **b**, Raman spectra of CN-550@C, CN-700@C, and CN-1000@C. **c**, **d**, N_2 physisorption isotherms (collected at 77 K) (c) of CN-550@C, CN-700@C, and CN-1000@C with the corresponding differential distribution of pore size plots calculated with non-linear density functional theory (d).

2.2 Electrochemical surface area

The electron and mass transport abilities of a material depend on its porosity and surface area[28]. Consequently, the porosity of CN@C was examined through nitrogen physisorption experiments shown in Fig. 2c and specific surface areas were determined according to the Brunauer–Emmett–Teller method[27]. CN-1000@C and CN-700@C have a specific surface area of 568 $m^2 \cdot g^{-1}$ and 555 $m^2 \cdot g^{-1}$, respectively, which are substantially higher than that of CN-550@C (294 $m^2 \cdot g^{-1}$), suggesting the presence of higher micropore contents in the materials at higher synthesis temperatures. All isotherms of the CN@C samples have the characteristics of type I, with a vertical N_2 uptake at the low-pressure range (P/P_0 < 0.01), suggesting the presence of narrow micropores in the synthesized catalysts[29]. The pore size distributions in Fig. 2d suggests that the materials primarily comprise micropores with diameters less than 2.0 nm, in agreement with our previous study[22].

A larger electrochemical surface area (ECSA) correlates with a higher accessibility and/or availability of catalytic sites for electrochemical reactions such as the ORR take place at the electrode/electrolyte interface[30, 31]. We used the double-layer capacitance (C_{dl}), which is directly proportionally related to the ECSA, to compare relative changes in surface area among the samples in our study[30, 31]. For this purpose, cyclic voltammograms were obtained for each catalyst within the non-Faradaic potential range of 0.8 to 1.1 V vs RHE at various scan rates ranging from 10 to 1000 $mV \cdot s^{-1}$. The obtained voltammograms are shown in Fig. 3a, and Supplementary Figs. S3c and S3e for CN-1000@C, CN-550@C, and CN-700@C, respectively. From the obtained voltammograms, the anodic and cathodic currents measured at a potential of 0.95 V vs RHE were extracted and graphed as a function of the scan rate as shown in Supplementary Figs. S3b, S3d, and S3f, respectively. The C_{dl} values were estimated using an allometric fit according to a previously reported procedure[32]. The fitting details are shown in Supplementary Table S1. The average value of C_{dl} is substantially larger for CN-1000@C (~ 0.46 mF) than those for CN-700@C (~ 0.26 mF) and CN-550@C (~ 0.01 mF), suggesting that CN-1000@C possesses a proportionally larger ECSA than the other two catalysts if the specific capacitance is independent of the synthesis treatment.

The correlation between specific surface area determined by gas physisorption and the C_{dl} provides insights into the ratio of the surface area involved in the electrochemical reaction (Fig. 3b). While the surface area trends were CN-1000@C > CN-700@C > CN-550@C for the two methods, a considerable difference between the C_{dl} values of CN-1000@C and CN-700@C is observed whereas their specific surface area are rather similar, suggesting that a larger portion of the surface area in CN-1000@C is in electrochemical contact with the electrolyte compared to CN-700@C, potentially leading to relatively superior ORR performance as discussed in the next section.

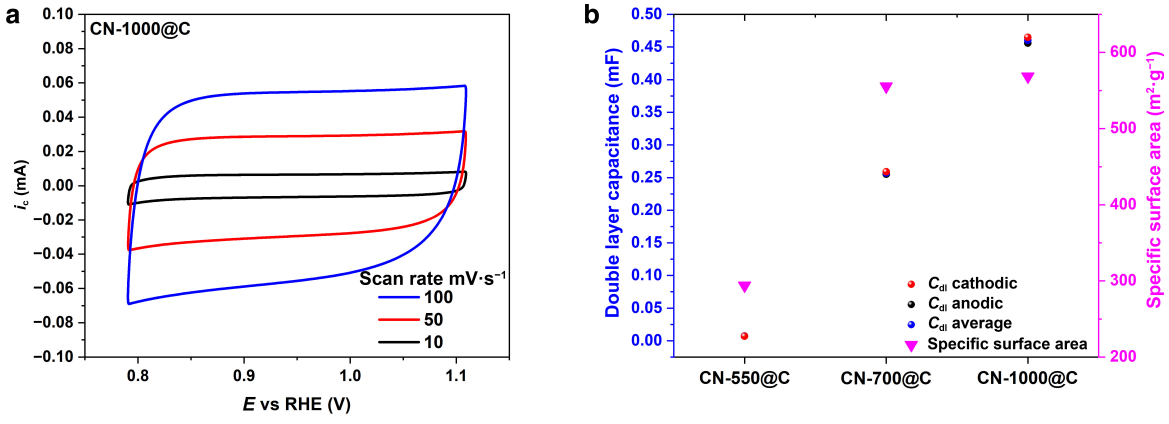

Fig. 3. Electrochemical and specific surface areas of CN@C materials. a, Cyclic voltammograms of CN-1000@C recorded at different scan rates from 10 to 100 mV·s^{-1} in the potential range of 0.8 to 1.1 V vs RHE. **b**, Comparison between double layer capacitance and specific surface area of CN@C materials.

2.3 Electrocatalytic activity for ORR

The electrocatalytic activity of the three CN@C samples towards the ORR was evaluated by rotating disk electrode (RDE) voltammetry using a O_2-saturated 0.1 M NaOH solution as the electrolyte. Voltammograms were recorded at a scan rate of 5 mV·s^{-1} and electrode rotation at 1600 rpm. Fig. 4a shows the obtained background-corrected voltammograms obtained with the three samples (an example of background correction of CN-1000@C is shown in Supplementary Fig. S3a). For each sample, three freshly prepared electrodes were measured under similar conditions. As shown for CN-1000@C in Supplementary Fig. S3b, the recorded voltammograms are highly overlapping, implying an excellent reproducibility of these measurements. To compare the electrocatalytic activity of the electrode in the kinetic-controlled voltammetric region, two parameters were determined, namely, the onset potential (E_{onset}), defined here as the potential at which the current density is up to 0.1 mA·cm^{-2}, and the potential at a current density of −1 mA·cm^{-2} (E_{-1}), normalized to the disk area[33, 34]. Linear sweep voltammetry (LSV) curves show that the CN-550@C electrode displays a poor activity with an E_{-1} value of 0.25 ± 0.02 V vs RHE and an E_{onset} of 0.73 ± 0.01 V vs RHE. Compared to CN-550@C, CN-700@C, and CN-1000@C exhibit enhanced electrode activity with E_{-1} of 0.59 ± 0.01 V and 0.69 ± 0.01 V vs RHE, respectively, and E_{onset} values of 0.83 ± 0.01 V and 0.88 ± 0.01 V, respectively. In addition, Fig. 4a shows that with increasing synthesis temperatures, the overall current density increased correspondingly: at a potential of 0.2 V vs RHE, the current density measured for the CN-1000@C electrode is −2.42 ± 0.02 mA·cm^{-2}, which is slightly higher than that of CN-700@C (−2.07 ± 0.02 mA·cm^{-2}) and two times higher than that of CN-550@C (−1.18 ± 0.04 mA·cm^{-2}). According to the comparison of the three samples, CN-1000@C is the most active in terms of overpotential and current density. The synergistic contribution of both a higher degree of graphitization and a larger surface area on CN-1000@C plays a vital role in the observed ORR activities. It is also possible that the hydrogen bonding of the water molecules confined within the pores of CN-1000 particles, which are more loosely bonded than for CN-550 and CN-700, facilitate the kinetics of the ORR reaction[23].

For the practical application toward the formation of H_2O_2 of ORR catalysts, excellent durability is required[18]. Therefore, we examined the stability by recording 100 cyclic voltammograms and then extracted the current at 0.4 V vs RHE which put more stress on the material and ensured the kinetics were maximized. Fig. 4b shows the currents recorded with the different CN@C materials as a function of the cycle number, relative to the current recorded during the first cycle. The CN-1000@C exhibits higher durability with the current in the system maintaining almost 95% by the end of the test compared to CN-700@C and CN-550@C, suggesting higher synthesis temperature impacts the stability favorably. After recording 100 cycles, LSVs were recorded to compare the activity before and after the stability test. As shown in Supplementary Fig. S4b, nearly no obvious shift was detected for the E_{onset}, while a negative shift of about 30 mV was observed for E_{-1}. These results show that synthesis temperature can be used to tune the stability of the material, however, practical applications require the stability to be tested at higher current densities and further efforts need to be directed into this direction.

To investigate the selectivity of CN-1000@C, which is critical to identify whether the reduction of O_2 is favored towards the production of H_2O_2, the K–L analysis was conducted[35]. LSVs were recorded at electrode rotation rates of 100, 400, 900, and 1600 rpm (Fig. 4c). As shown in Supplementary Fig. S4c, the measurements show a high reproducibility. Fig. 4d shows the K–L plot derived from the recorded voltammograms, showing a linear relationship between the inverse of the current density ($1/j$) and the negative of the square root of the scan rate ($\omega^{-0.5}$), which suggested a first-order dependence of the O_2 concentration on the CN-1000@C electrode[36]. To investigate the catalytic ORR pathways of CN-1000@C, a linear fit of the K–L plots was adopted. The number of electrons transferred (n) were calculated from the slopes of the K–L plots as 2.4, 2.2, 2.2, 2.2, and 2.3 for electrode potentials of 0.7, 0.675, 0.65, 0.625, and 0.6 V vs RHE, respectively, according to Eq. (3). This analysis revealed that CN-1000@C favors the two-electron transfer pathway during the ORR process, indicating that CN-1000@C has high selectivity towards the formation of H_2O_2. In recent years, surface-functionalized carbon-based materials, particularly those with oxygen-containing groups, have emerged as promising and cost-effective candidates for 2e$^-$ ORR catalysts[37]. Conversely, carbon catalysts lacking surface oxygen functional groups, or oxygen-free carbon catalysts, demonstrate low H_2O_2 selectivity[38]. Therefore, the existence of surface oxygen functional groups while maintaining a high degree of graphitization in CN-1000@C is certainly beneficial to the selective production of peroxide. Note that the CN-1000 also has a larger ECSA, largely enhancing the ORR performance in terms of current density, which

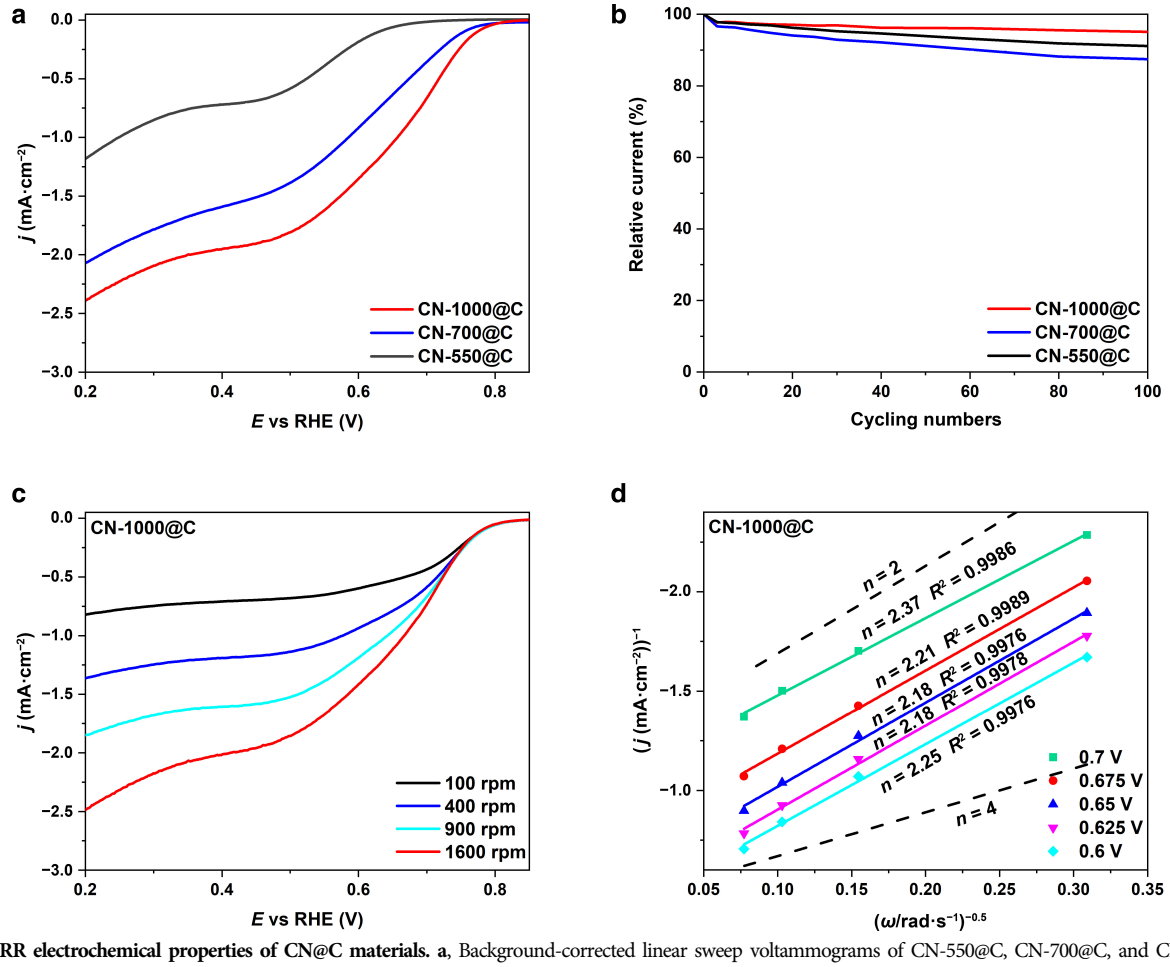

Fig. 4. ORR electrochemical properties of CN@C materials. a, Background-corrected linear sweep voltammograms of CN-550@C, CN-700@C, and CN-1000@C recorded at a scan rate of 5 mV·s^{-1} with electrode rotation rate of 1600 rpm. **b**, Relative current as a function of time for the evaluation of the stability of CN-550@C, CN-700@C, and CN-1000@C determined by recording 100 cyclic voltammograms at scan rate of 50 mV·s^{-1}. **c**, Background-corrected linear sweep voltammograms of CN-1000@C recorded at a scan rate of 5 mV·s^{-1} with electrode rotation rates of 100, 400, 900, and 1600 rpm. **d**, The fitted Koutecký–Levich plots of CN-1000@C at different electrode potentials for the determination of the number of electrons transferred; plots corresponding to the theoretical n = 2 and n = 4 are shown to facilitate visual comparison. All measurements were performed using an O_2-saturated 0.1 M NaOH solution as the electrolyte.

Table 1 Electrocatalytic ORR performance of metal-free N-doped carbons. *Electrode potential values E_{-1} (corresponding to a current density of −1 mA·cm^{-2}) were estimated from the voltammograms reported in the corresponding references. The onset potential (E_{onset}), is defined here as the potential at which the current density reaches 0.1 mA·cm^{-2}.

Catalyst	Electrolyte	Scan rate (mV·s^{-1})	E_{onset}* (V vs RHE)	E_{-1}* (V vs RHE)	Average number of electrons transferred	Ref.
CN-1000@C	0.1 M NaOH	5	0.88	0.69	2.2	This work
a-C:N 900	0.1 M KOH	10	0.77	0.63	2.4	[40]
NCNC700/900	0.1 M KOH	10	0.85	0.77	3.3	[41]
CCa	0.1 M KOH	10	0.90	0.8	3.8	[42]
NHCS-1000	0.1 M KOH	10	0.85	0.77	4.0	[43]
Baytubes-PPy	0.1 M KOH	5	0.90	0.4	3.3	[44]
NC-900	0.1 M KOH	10	0.97	0.85	3.9	[45]
PDMC-800	0.1 M KOH	5	0.71	0.71	2.7	[46]
COF-JLU23	0.1 M KOH	10	0.99	0.67	3.7	[47]

may be related to a more hierarchical microporosity due to the higher condensation temperature. The microporosity should not be overlooked when enriching the porous carbon with N functionalities[39]. As a whole, there is a trade-off between nitrogen content, which is favorable for O_2 adsorption, and high-temperature annealing which favor the formation of smaller pores, a more graphitic structure and a higher amount of surface oxygen functional groups, with hence a higher electrical conductivity. It appears that the HAT-CN-1000 material offers the best electrochemical performance despite a smaller N content, however these sites are still very important as purely carbonaceous particles are not active for ORR.

The ORR performance in terms of activity and number of electrons transferred of a few selected recently reported N-doped metal-free catalysts is listed in Table 1 for benchmarking the CN-1000@C samples. While other metal-free catalysts clearly exhibit lower ORR overpotentials than CN-1000@C, the average electrons transferred number of the latter is the closest to two (n = 2.2), indicating a higher selectivity towards the two-electron transfer pathway that may theoretically lead to an 89% peroxide yield. Thus, the high $2e^-$ selectivity of this material indicates the potential suitability of this class of electrocatalysts for H_2O_2 synthesis. Further improvements of CN@C electrocatalytic activity and stability are though required to become an alternative material to palladium hydrogenation catalysts with significantly lower costs.

3 Conclusions

A series of nitrogen-rich CN@C-type materials was synthesized at different temperatures for electrochemical oxygen reduction to produce hydrogen peroxide. A metal-free template synthesis method of CN@C was established to generate catalytically active sites for ORR with a large specific surface area (> 500 $m^2 \cdot g^{-1}$) that is also electrochemically active. The ORR performance of the synthesized materials was evaluated using rotating disk electrode voltammetry. CN-1000@C shows excellent ORR selectivity of 89% towards the production of H_2O_2 in alkaline media, ORR onset of 0.88 V vs RHE and about 95% current retention, thus it outperforms CN-700@C and CN-550@C and many previously reported carbon-based electrocatalysts. The improvement is attributed to a good balance between the nitrogen content and degree of graphitization, controlled by the synthesis temperature, as well as the addition of a carbon support to increase their conductivity. This work demonstrates that nitrogen-rich carbons generated by a HAT monomer-induced template synthesis process are good candidates for highly selective two-electron ORR pathway for H_2O_2 production.

4 Experimental section

4.1 Materials synthesis

Hexaazatriphenylenehexacarbonitrile (HAT-CN) was prepared in accordance with the methods reported in previous literature[22, 48]. Commercial-grade carbon cloths (Kynol 5092-CC) were sourced from Kynol Europa GmbH and pulverized by Impact Ball Mill (Pulverisette 23, Fritsch GmbH) at 3000 rpm for 20 min to obtain the Kynol powder. CN@C carbons were prepared through post-treatment and calcination of Kynol powder with HAT-CN. In a typical procedure, 100 mg of HAT-CN was dissolved in 400 µL of dimethylformamide (DMF, > 99 %, Sigma Aldrich) by sonication. 100 mg of Kynol powder was subsequently mixed with the resulting HAT-CN solution, where the mixture was then dried under vacuum at 60 °C for 12 h. HAT@C carbons were synthesized by calcining the composite material in a horizontal tubular furnace under a nitrogen flow. Specifically, the temperature was initially increased to 60 °C at a rate of 4 °C·min^{-1} and held for 0.5 h. Afterwards, the temperature was raised to the target temperatures of either 550, 700, or 1000 °C at a rate of 4 °C·min^{-1} and held for 1 h. The resulting materials were denoted as HAT@C-550, HAT@C-700, and HAT@C-1000, according to their respective condensation temperatures.

4.2 Material characterizations

Transmission electron microscopy was performed on a JEOL-2100 transmission electron microscopy (JEOL, GmbH, Eching, Germany) at an acceleration voltage of 200 kV. Scanning electron microscopy was carried out on a LEO 1550-Gemini microscope operating at 3.00 kV. A platinum layer was sputtered onto the samples to enhance surface conductivity. Energy-dispersive X-ray analysis was performed using a Link ISIS-300 system (Oxford Microanalysis Group), equipped with a Si(Li) detector and an energy resolution of 133 eV. Powder X-ray diffraction (PXRD) patterns were collected using a Bruker D8 Advance diffractometer, equipped with a scintillation counter detector and Cu Kα radiation (λ = 0.15184 nm), with a 2θ step size of 0.02°. Raman spectra were recorded using a Witec (focus innovations) Raman Microscope operating with an objective (Nikon, 10x/0.25, ∞/-WD 6.1) and an excitation wavelength of 532 nm with an intensity of 3.5 mW. The nitrogen sorption isotherms were measured with a Belsorp Max automatic volumetric adsorption system at liquid nitrogen temperature (77 K) using N_2 as the probe gas after a degassing process at 120 °C for 12 h under vacuum. The specific surface areas and pore size distribution were obtained by using the Brunauer–Emmett–Teller test.

4.3 Electrochemical measurements

All electrochemical measurements were performed in a standard three-electrode cell using a Reference 600+ potentiostat (Gamry) and an RRDE-3A rotator (ALS Inc.). A 4 mm diameter glassy carbon (GC) rotating disk electrode, coated with catalyst ink, served as the working electrode. To coat the working electrode, catalyst deposition was done by drop-casting 2.8 µL catalyst ink and then dried naturally under air. The ink was prepared by dispersing 5 mg·mL^{-1} of catalyst through 15 min of sonication in a water-ethanol mixture (1:1 volume ratio) with 2 vol.% Nafion solution (~ 5% Nafion in a mixture of alcohols, Sigma-Aldrich) as a binder. The total catalyst loading on the GC electrode was 198 µg·cm^{-2}. Hg|HgO (ALS Inc.) filled with 1 M NaOH solution and a graphite rod served as the reference electrode and the counter electrode, respectively. All the electrochemical experiments were conducted in O_2-saturated or Ar-saturated 0.1 M NaOH solution (Sigma-Aldrich) at room temperature. Before each test, the electrolyte was fully purged with argon or oxygen for 30 min. A continuous flow of the appropriate gas is kept near the electrolyte surface during the measurements to maintain gas saturation.

Before the ORR measurements, 10 cyclic voltammograms were recorded with the catalyst-modified electrodes at a scan rate of 100 mV·s^{-1} in the potential range from 0.2 to −0.4 V vs Hg|HgO|NaOH. A stable voltammetric response was noted by the end of this conditioning step. Subsequently, electrochemical impedance spectra were collected in the frequency range from 100 kHz to 1 Hz with an AC amplitude of 10 mV (RMS) to determine the uncompensated resistance (R_u), and later correct the measured data ($E_{measured}$) by the iR_u-drop according to Supplementary Eq. S1, where $i_{measured}$ represents the recorded current. All potentials were adjusted to the RHE scale by measuring the open circuit voltage between an RHE electrode (Gaskatel) and the reference electrode for 10 min at the beginning of each measurement day. The last value recorded (V_{RE}) was applied to calculate the potentials vs RHE according to Eq. 1. The average value obtained for different experiment days was 0.89 ± 0.01 V. The obtained R_u values were in average 77 ± 5 Ω for CN-1000@C, CN-700@C, and CN-550@C,

respectively.

$$E_{corrected} = E_{measured} + V_{RE} - i_{measured}R_u \quad (1)$$

To investigate the ORR activity, linear sweep voltammograms were recorded in the potential range from 0.2 to −0.8 vs Hg|HgO|NaOH at a scan rate of 5 mV·s^{-1} and rotation rate of 1600 rpm. All activity measurements were conducted in triplicate using freshly prepared working electrodes to evaluate the reproducibility of the results (Supplementary Fig. S3b). A supplementary voltammogram was obtained in an O_2-free electrolyte saturated with Ar at the same scan rate to establish the background current, which was subsequently subtracted from the recorded voltammograms. (Supplementary Fig. S3a).

To investigate the ORR stability, 100 cyclic voltammograms were recorded with the catalyst-modified electrodes at a scan rate of 50 mV·s^{-1} in the potential range from 0.2 to −0.8 V vs Hg|HgO|NaOH at a rotation rate of 1600 rpm. Then the current density values at 0.4 V vs RHE were graphed as a function of the corresponding number of cycles.

Cyclic voltammetry (CV) was conducted to measure the electrochemical double-layer capacitance in the non-Faradaic potential window from 0.2 to −0.4 V vs Hg|HgO|NaOH at various scan rates (10, 50, 100, 500, and 1000 mV·s^{-1}). The fitting model is derived from an allometric regression, where Y represents the current and X denotes the scan rate, respectively. The slope b corresponds to the capacitance while an exponent α is associated to deviations from linearity (Eq. 2). [32]

$$Y = bX^{\alpha} \quad (2)$$

To assess the selectivity of the catalysts, RDE voltammetry was conducted at different rotation speeds, varying from 100 to 1600 rpm, with a sweep rate of 5 mV·s^{-1}. This experiment was done in duplicate for each catalyst to ensure that the results are reproducible (Supplementary Fig. S3c). The Koutechý–Levich equation (Eq. 3) was adopted to determine the number of electrons transfer during ORR.

$$1/J = 1/(0.62nFC_0D_0^{2/3}V^{-1/6}\omega^{1/2}) + 1/J_K \quad (3)$$

where J represents the measured current density, J_K is the kinetic-limited current density, ω is the angular velocity of the disk electrode, n denotes the electron transfer number, F is the Faraday constant (96,485 C·mol^{-1}), C_0 is the bulk concentration of O_2 (1.2×10^{-6} mol·cm^{-3}), D_0 refers to the diffusion coefficient of O_2 in 0.1 M KOH (1.9×10^{-5} cm^2·s^{-1}), and V is the kinematic viscosity of the electrolyte (0.01 cm^2·s^{-1})[49].

The peroxide yield, X, in percent was calculated according to Eq. 4:

$$X = 2 \cdot 100\% - (2-4)/100\% \cdot n \quad (4)$$

References

[1] Brillas, E.; Sirés, I.; Oturan, M. A. Electro-fenton process and related electrochemical technologies based on fenton's reaction chemistry. *Chem. Rev.* **2009**, *109*, 6570–6631.

[2] Wang, K.; Huang, J. H.; Chen, H. X.; Wang, Y.; Song, S. Q. Recent advances in electrochemical 2e oxygen reduction reaction for on-site hydrogen peroxide production and beyond. *Chem. Commun.* **2020**, *56*, 12109–12121.

[3] Wang, N.; Ma, S. B.; Zuo, P. J.; Duan, J. Z.; Hou, B. R. Recent progress of electrochemical production of hydrogen peroxide by two-electron oxygen reduction reaction. *Adv. Sci.* **2021**, *8*, 2100076.

[4] Campos-Martin, J. M.; Blanco-Brieva, G.; Fierro, J. L. G. Hydrogen peroxide synthesis: An outlook beyond the anthraquinone process. *Angew. Chem., Int. Ed.* **2006**, *45*, 6962–6984.

[5] Wang, Y. L.; Waterhouse, G. I. N.; Shang, L.; Zhang, T. R. Electrocatalytic oxygen reduction to hydrogen peroxide: From homogeneous to heterogeneous electrocatalysis. *Adv. Energy Mater.* **2021**, *11*, 2003323.

[6] Dan, M.; Zhong, R. Y.; Hu, S. Y.; Wu, H. X.; Zhou, Y.; Liu, Z. Q. Strategies and challenges on selective electrochemical hydrogen peroxide production: Catalyst and reaction medium design. *Chem Catal.* **2022**, *2*, 1919–1960.

[7] Xia, C.; Kim, J. Y.; Wang, H. T. Recommended practice to report selectivity in electrochemical synthesis of H_2O_2. *Nat. Catal.* **2020**, *3*, 605–607.

[8] Zheng, Z. K.; Ng, Y. H.; Wang, D. W.; Amal, R. Epitaxial growth of Au–Pt–Ni nanorods for direct high selectivity H_2O_2 production. *Adv. Mater.* **2016**, *28*, 9949–9955.

[9] Chang, Q. W.; Zhang, P.; Mostaghimi, A. H. B.; Zhao, X. R.; Denny, S. R.; Lee, J. H.; Gao, H. P.; Zhang, Y.; Xin, H. L.; Siahrostami, S. et al. Promoting H_2O_2 production via 2-electron oxygen reduction by coordinating partially oxidized Pd with defect carbon. *Nat. Commun.* **2020**, *11*, 2178.

[10] Yang, S.; Verdaguer-Casadevall, A.; Arnarson, L.; Silvioli, L.; Čolić, V.; Frydendal, R.; Rossmeisl, J.; Chorkendorff, I.; Stephens, I. E. L. Toward the decentralized electrochemical production of H_2O_2: A focus on the catalysis. *ACS Catal.* **2018**, *8*, 4064–4081.

[11] Jiang, Y. Y.; Ni, P. J.; Chen, C. X.; Lu, Y. Z.; Yang, P.; Kong, B.; Fisher, A.; Wang, X. Selective electrochemical H_2O_2 production through two-electron oxygen electrochemistry. *Adv. Energy Mater.* **2018**, *8*, 1801909.

[12] Priyadarsini, A.; Mallik, B. S. Effects of doped N, B, P, and S atoms on graphene toward oxygen evolution reactions. *ACS Omega* **2021**, *6*, 5368–5378.

[13] Choi, C. H.; Lim, H. K.; Chung, M. W.; Chon, G.; Sahraie, N. R.; Altin, A.; Sougrati, M. T.; Stievano, L.; Oh, H. S.; Park, E. S. et al. The Achilles' heel of iron-based catalysts during oxygen reduction in an acidic medium. *Energy Environ. Sci.* **2018**, *11*, 3176–3182.

[14] Ehlert, C.; Piras, A.; Schleicher, J.; Gryn'ova, G. Metal-free molecular catalysts for the oxygen reduction reaction: Electron affinity as an activity descriptor. *J. Phys. Chem. Lett.* **2023**, *14*, 476–480.

[15] Wu, B.; Meng, H. B.; Morales, D. M.; Zeng, F.; Zhu, J. J.; Wang, B.; Risch, M.; Xu, Z. J.; Petit, T. Nitrogen-rich carbonaceous materials for advanced oxygen electrocatalysis: Synthesis, characterization, and activity of nitrogen sites. *Adv. Funct. Mater.* **2022**, *32*, 2204137.

[16] Zhang, W. Y.; Zhan, S. Q.; Qin, Q.; Heil, T.; Liu, X. Y.; Hwang, J.; Ferber, T. H.; Hofmann, J. P.; Oschatz, M. Electrochemical generation of catalytically active edge sites in C_2N-type carbon materials for artificial nitrogen fixation. *Small* **2022**, *18*, 2204116.

[17] Kazakova, M. A.; Koul, A.; Golubtsov, G. V.; Selyutin, A. G.; Ishchenko, A. V.; Kvon, R. I.; Kolesov, B. A.; Schuhmann, W.; Morales, D. M. Nitrogen and oxygen functionalization of multi-walled carbon nanotubes for tuning the bifunctional oxygen reduction/oxygen evolution performance of supported FeCo oxide nanoparticles. *ChemElectroChem* **2021**, *8*, 2803–2816.

[18] Zhang, L. P.; Niu, J. B.; Dai, L. M.; Xia, Z. H. Effect of microstructure of nitrogen-doped graphene on oxygen reduction activity in fuel cells. *Langmuir* **2012**, *28*, 7542–7550.

[19] Dai, L. M.; Xue, Y. H.; Qu, L. T.; Choi, H. J.; Baek, J. B. Metal-free

catalysts for oxygen reduction reaction. *Chem. Rev.* **2015**, *115*, 4823–4892.

[20] Perovic, M.; Qin, Q.; Oschatz, M. From molecular precursors to nanoparticles-tailoring the adsorption properties of porous carbon materials by controlled chemical functionalization. *Adv. Funct. Mater.* **2020**, *30*, 1908371.

[21] Borchardt, L.; Zhu, Q. L.; Casco, M. E.; Berger, R.; Zhuang, X. D.; Kaskel, S.; Feng, X. L.; Xu, Q. Toward a molecular design of porous carbon materials. *Mater. Today* **2017**, *20*, 592–610.

[22] Walczak, R.; Kurpil, B.; Savateev, A.; Heil, T.; Schmidt, J.; Qin, Q.; Antonietti, M.; Oschatz, M. Template- and metal-free synthesis of nitrogen-rich nanoporous "noble" carbon materials by direct pyrolysis of a preorganized hexaazatriphenylene precursor. *Angew. Chem., Int. Ed.* **2018**, *57*, 10765–10770.

[23] Wu, B.; Amargianou, F.; Förster, J. D.; Pöhlker, C.; Rauch, T. G.; Wong, D.; Schulz, C.; Seidel, R.; Weigand, M.; Oschatz, M. et al. Water confinement in nitrogen-rich nanoporous carbon materials revealed by *in situ* scanning transmission X-ray microscopy. *Adv. Funct. Mater.*, **2024**, *34*, 2406528.

[24] Hwang, J.; Zhang, W. Y.; Youk, S.; Schutjajew, K.; Oschatz, M. Understanding structure-property relationships under experimental conditions for the optimization of lithium-ion capacitor anodes based on all-carbon-composite materials. *Energy Technol.* **2021**, *9*, 2001054.

[25] Wang, X. F.; Liu, T. Y.; Li, H. T.; Han, C.; Su, P. P.; Ta, N.; Jiang, S. P.; Kong, B.; Liu, J.; Huang, Z. G. Balancing mass transfer and active sites to improve electrocatalytic oxygen reduction by B,N codoped C nanoreactors. *Nano Lett.* **2023**, *23*, 4699–4707.

[26] Wang, L.; Ambrosi, A.; Pumera, M. "Metal-free" catalytic oxygen reduction reaction on heteroatom-doped graphene is caused by trace metal impurities. *Angew. Chem., Int. Ed*. **2013**, *52*, 13818–13821.

[27] Sakaushi, K.; Fellinger, T. P.; Antonietti, M. Bifunctional metal-free catalysis of mesoporous noble carbons for oxygen reduction and evolution reactions. *ChemSusChem* **2015**, *8*, 1156–1160.

[28] Banerjee, S.; Anayah, R. I.; Gerke, C. S.; Thoi, V. S. From molecules to porous materials: Integrating discrete electrocatalytic active sites into extended frameworks. *ACS Cent. Sci.* **2020**, *6*, 1671–1684.

[29] Storck, S.; Bretinger, H.; Maier, W. F. Characterization of micro- and mesoporous solids by physisorption methods and pore-size analysis. *Appl. Catal. A: Gen.* **1998**, *174*, 137–146.

[30] Connor, P.; Schuch, J.; Kaiser, B.; Jaegermann, W. The determination of electrochemical active surface area and specific capacity revisited for the system MnO_x as an oxygen evolution catalyst. *Z. Phys. Chem.* **2020**, *234*, 979–994.

[31] Han, G. Q.; Liu, Y. R.; Hu, W. H.; Dong, B.; Li, X.; Shang, X.; Chai, Y. M.; Liu, Y. Q.; Liu, C. G. Crystallographic structure and morphology transformation of MnO_2 nanorods as efficient electrocatalysts for oxygen evolution reaction. *J. Electrochem. Soc.* **2016**, *163*, H67–H73.

[32] Morales, D. M.; Risch, M. Seven steps to reliable cyclic voltammetry measurements for the determination of double layer capacitance. *J. Phys.: Energy* **2021**, *3*, 034013.

[33] Mayrhofer, K. J. J.; Strmcnik, D.; Blizanac, B. B.; Stamenkovic, V.; Arenz, M.; Markovic, N. M. Measurement of oxygen reduction activities via the rotating disc electrode method: From Pt model surfaces to carbon-supported high surface area catalysts. *Electrochim. Acta* **2008**, *53*, 3181–3188.

[34] Chen, W. L.; Xiang, Q.; Peng, T.; Song, C. Y.; Shang, W.; Deng, T.; Wu, J. B. Reconsidering the benchmarking evaluation of catalytic activity in oxygen reduction reaction. *iScience* **2020**, *23*, 101532.

[35] Jeon, I. Y.; Zhang, S.; Zhang, L. P.; Choi, H. J.; Seo, J. M.; Xia, Z. H.; Dai, L. M.; Baek, J. B. Edge-selectively sulfurized graphene nanoplatelets as efficient metal-free electrocatalysts for oxygen reduction reaction: The electron spin effect. *Adv. Mater.* **2013**, *25*, 6138–6145.

[36] Unni, S. M.; Ramadas, S.; Illathvalappil, R.; Bhange, S. N.; Kurungot, S. Surface-modified single wall carbon nanohorn as an effective electrocatalyst for platinum-free fuel cell cathodes. *J. Mater. Chem. A* **2015**, *3*, 4361–4367.

[37] Liu, X. E.; Dai, L. M. Carbon-based metal-free catalysts. *Nat. Rev. Mater.* **2016**, *1*, 16064.

[38] Xia, C.; Xia, Y.; Zhu, P.; Fan, L.; Wang, H. T. Direct electrosynthesis of pure aqueous H_2O_2 solutions up to 20% by weight using a solid electrolyte. *Science* **2019**, *366*, 226–231.

[39] Iglesias, D.; Giuliani, A.; Melchionna, M.; Marchesan, S.; Criado, A.; Nasi, L.; Bevilacqua, M.; Tavagnacco, C.; Vizza, F.; Prato, M. et al. N-doped graphitized carbon nanohorns as a forefront electrocatalyst in highly selective O_2 reduction to H_2O_2. *Chem* **2018**, *4*, 106–123.

[40] Behan, J. A.; Mates-Torres, E.; Stamatin, S. N.; Domínguez, C.; Iannaci, A.; Fleischer, K.; Hoque, M. K.; Perova, T. S.; García-Melchor, M.; Colavita, P. E. Untangling cooperative effects of pyridinic and graphitic nitrogen sites at metal-free N-doped carbon electrocatalysts for the oxygen reduction reaction. *Small* **2019**, *15*, 1902081.

[41] Chen, S.; Bi, J. Y.; Zhao, Y.; Yang, L. J.; Zhang, C.; Ma, Y. W.; Wu, Q.; Wang, X. Z.; Hu, Z. Nitrogen-doped carbon nanocages as efficient metal-free electrocatalysts for oxygen reduction reaction. *Adv. Mater.* **2012**, *24*, 5593–5597.

[42] Ferrero, G. A.; Fuertes, A. B.; Sevilla, M.; Titirici, M. M. Efficient metal-free N-doped mesoporous carbon catalysts for ORR by a template-free approach. *Carbon* **2016**, *106*, 179–187.

[43] Zhou, T. S.; Zhou, Y.; Ma, R. G.; Zhou, Z. Z.; Liu, G. H.; Liu, Q.; Zhu, Y. F.; Wang, J. C. Nitrogen-doped hollow mesoporous carbon spheres as a highly active and stable metal-free electrocatalyst for oxygen reduction. *Carbon* **2017**, *114*, 177–186. [44] Zhao, A. Q.; Masa, J.; Muhler, M.; Schuhmann, W.; Xia, W. N-doped carbon synthesized from N-containing polymers as metal-free catalysts for the oxygen reduction under alkaline conditions. *Electrochim. Acta* **2013**, *98*, 139–145.

[44] Yang, M.; Liu, Y. J.; Chen, H. B.; Yang, D. G.; Li, H. M. Porous N-doped carbon prepared from triazine-based polypyrrole network: A highly efficient metal-free catalyst for oxygen reduction reaction in alkaline electrolytes. *ACS Appl. Mater. Interfaces* **2016**, *8*, 28615–28623.

[45] Silva, R.; Voiry, D.; Chhowalla, M.; Asefa, T. Efficient metal-free electrocatalysts for oxygen reduction: Polyaniline-derived N-and O-doped mesoporous carbons. *J. Am. Chem. Soc.* **2013**, *135*, 7823–7826.

[46] Jia, J.; Li, J. L.; Ma, S.; Zhang, Z. W.; Liu, X. M. Metal-free covalent organic frameworks for electrocatalytic oxygen reduction reaction. *Macromol. Rapid Commun.* **2023**, *44*, 2200717.

[47] Yan, R. Y.; Leus, K.; Hofmann, J. P.; Antonietti, M.; Oschatz, M. Porous nitrogen-doped carbon/carbon nanocomposite electrodes enable sodium ion capacitors with high capacity and rate capability. *Nano Energy* **2020**, *67*, 104240.

[48] Jin, Z. P.; Nie, H. G.; Yang, Z.; Zhang, J.; Liu, Z.; Xu, X. J.; Huang, S. M. Metal-free selenium doped carbon nanotube/graphene networks as a synergistically improved cathode catalyst for oxygen reduction reaction. *Nanoscale* **2012**, *4*, 6455–6460.

Data availability

All data required to support the conclusions of this paper are

included in the manuscript and the Supplementary Information. Further data related to this research can be requested from the corresponding author.

Acknowledgments

This work was supported by the Volkswagen Foundation (Freigeist Fellowship No. 89592) and CSC scholarship (No. 201904910594). M.O. acknowledges funding by the European Union (ERC, CILCat, project number 101040394). The views and opinions presented are solely those of the author(s) and do not necessarily represent those of the European Union or the European Research Council Executive Agency. The European Union and the granting authority are not liable for any statements made.

Author contributions

B.W. and D.M.M. performed the electrochemical experiments and wrote the manuscript. B.W. collected the data and carried out XRD and Raman measurements. M.L. synthesized the samples under the supervision of M.O., D.J.X, P.F., and Y.L. performed and analysed TEM, SEM, and BET measurements. T.P., M.O., and M.R. analysed the data and revised the manuscript. T.P. initiated and supervised the whole project. All the authors discussed the results and assisted during the manuscript preparation.

Competing interests

The authors have no competing interests to declare that are relevant to the content of this article. Author Martin Oschatz is the Associate Editor of this journal, but he is not involved in the peer-review or decision of this article.

Additional Information

Supplementary Information The online version contains supplementary material available at https://doi.org/10.26599/CF.2024.9200022.